Article

Hybridization of a RoR HPP with a BESS—The XFLEX HYDRO Vogelgrun Demonstrator

Serdar Kadam [1,*]**, Wolfgang Hofbauer** [1]**, Stefan Lais** [2]**, Magdalena Neuhauser** [3]**, Erich Wurm** [1]**, Luisa Fernandes Lameiro** [1]**, Yves-Marie Bourien** [4]**, Grégory Païs** [4]**, Jean-Louis Drommi** [5]**, Christophe Nicolet** [6]**, Christian Landry** [6]**, Matthieu Dreyer** [6]**, Carme Valero** [7]**, Alexandre Presas** [7] **and David Valentin** [7]

1 Andritz Hydro GmbH, Eibesbrunnergasse 20, 1120 Vienna, Austria
2 Andritz Hydro AG, Address Obernauerstrasse 4, 6010 Kriens, Switzerland
3 Andritz Hydro AG, Rue des Deux Gares 6, 1800 Vevey, Switzerland
4 Campus INES, Université Grenoble Alpes, CEA, LITEN, 73375 Le Bourget du Lac, France
5 Electricité de France, Hydro Engineering Center, Savoie Technolac, 73373 Le Bourget du Lac, France
6 Power Vision Engineering Sàrl, Rue des Jordils 40, 1025 St-Sulpice, Switzerland
7 Center for Industrial Diagnostics and Fluid Dynamics (CDIF), Polytechnic University of Catalonia (UPC), Av. Diagonal, 647, ETSEIB, 08028 Barcelona, Spain
* Correspondence: serdar.kadam@andritz.com

Abstract: In the XFLEX HYDRO Vogelgrun demonstrator, a run-of-river hydropower plant, the hybridization of one turbine-generator unit with a battery energy storage system is being investigated. This paper describes the integration methodology of the hybrid control algorithm without replacing the existing speed governor of the unit. Furthermore, the comparison of the performances of a non-hybrid and hybrid unit is discussed, and first experiences gained during the operation and monitoring of the hybrid operating mode are presented.

Keywords: hybridization; run-of-river; flexibility; primary control; FCR; battery energy storage system

1. Introduction

With the phaseout of thermal power plants and integration of variable renewables such as wind and PV, the demand for operational flexibility in power systems changes and increases. Therefore, the capability of existing hydropower plants to offer such flexibilities, and to even extend it, is becoming even more important. The worldwide installed hydropower capacity hit 1369 GW in 2021. An additional 26 GW of capacity was added in 2021, including pumped storage. The total installed pumped-storage capacity exceeded 165 GW. In that year, around 4250 TWh of electricity was generated from hydropower, according to [1]. In [2], the hydropower project pipeline from 2022 to 2037 is described. According to [2], new installations of 651 GW (of which 136 GW are pumped storage) are foreseen. Hence, the existing hydropower fleet plays not only an important role in carbon-free power generation but also in the integration of wind and PV by providing flexibility.

In [3], the contribution of hydropower to grid resilience is described. In particular, it is noted that hydropower plants can enhance a system's response and recovery attributes by including a wide band of frequency ride-through ability. Further, it is mentioned that hydropower plants are an important resource for inertial and governor response during extreme events. To increase the operational flexibility of hydropower plants (HPP) even further, existing limitations, which are defined by the HPP type (e.g., run-of-river, pumped-storage hydro, reservoir type etc.), must be overcome by means of technological improvements. At the same time, other regulations (e.g., the water framework directive) must be respected at all times.

In the Horizon 2020-funded XFLEX HYDRO project [4], a consortium of 19 partners demonstrates different types of HPPs, including how more flexibility can be provided

to enable the integration of even more intermittent renewables. In total, innovations are demonstrated at seven HPP locations in Portugal, France and Switzerland. Demonstrated technologies include a conversion to variable speed, operation with hydraulic short circuit and a hydro–battery hybrid system. At the hydro–battery hybrid system, the benefits of providing FCR with a run-of-river power plant and a BESS are studied.

In [5], the load-frequency control process of the ENTSO-E synchronous area is described (Figure 1). Whenever an imbalance between supply and demand occurs, the frequency starts to deviate from its controlled value (e.g., 50 Hz). A drift of the frequency is stabilized by means of the frequency containment process within permissible limits. After that, the frequency restoration process is activated in the load-frequency control (LFC) areas where the disturbance occurred. This process ensures that the frequency is restored to the frequency setpoint. European TSOs cover the FCR demand via a cooperation [5]. The total demand of FCR within this cooperation is 1531 MW (approximately 514 MW in France and 593 MW in Germany) [6].
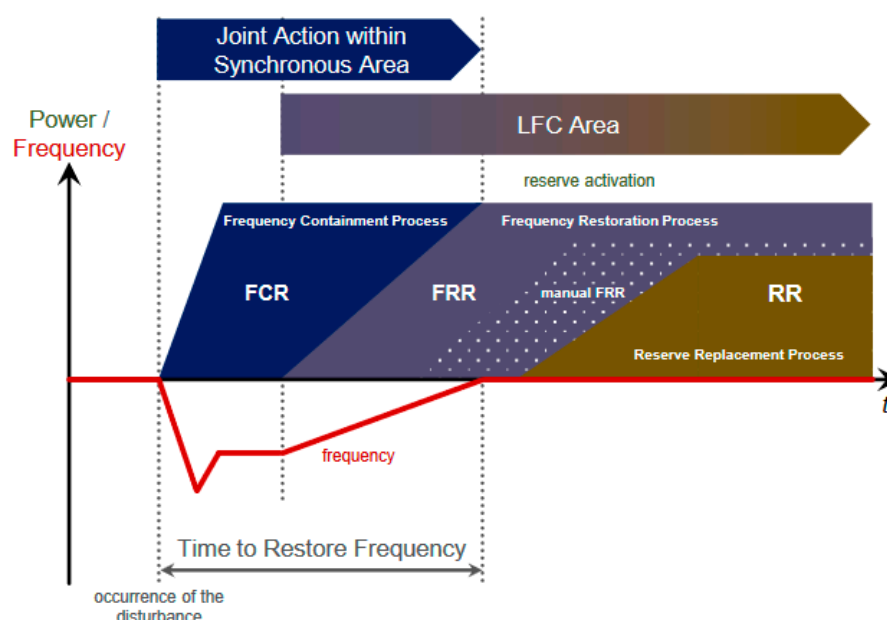

Figure 1. Dynamic hierarchy of load-frequency control processes [7].

To deliver FCR, the contracted active power has to be provided for full activation (200 mHz) within 30 s [8,9]. The optimization and sizing for stand-alone BESS were, for example, discussed in [10–12]. A practical approach to sizing BESS for FCR provision was proposed in [13], in particular, for power systems with a large wind power penetration level. In [10], a general formulation was derived to obtain the minimum size of a stand-alone BESS. To provide 1 MW of FCR with a stand-alone BESS, a minimum BESS size of 1.6 MW/1.6 MWh was obtained. Hence, reserves in terms of sizing must be considered to comply with FCR requirements and ensure a sufficient service life to reach economic viability. An alternative to providing FCR with a stand-alone BESS, or any type of generation technology, is to use a hybrid system. With a hybrid system, two different systems can be combined in such a way that FCR requirements are fulfilled. Thereby, both systems are used to the full extent and according to their capabilities.

In [14], it was found that hybridizing the hydropower plant can generate additional revenue while simultaneously enabling more environmentally friendly operations and reducing the overall ramping mileage (sum of up and down ramping) of the turbines to approximately 1/5th of the mileage from hydropeaking operations.

The advantages of operating a BESS with a pumped-storage plant to increase its flexibility based on live test results were described in [15]. The authors summarize that the combination of three pumped-storage units and a BESS substantially increases the

flexibility of the operator's FCR reserve pool. This is obtained with two features: fast ramping with the BESS and large autonomy of pumped hydro.

In [16,17], the advantages of combining run-of-river (RoR) hydropower plants with BESS is presented. The analysis shows that the movement of guide vanes and runner blades can be reduced significantly with a properly sized BESS.

At the XFLEX HYDRO Vogelgrun demonstrator, a run-of-river power plant, frequency containment reserve (FCR) is provided with a hydro–battery hybrid. In doing so, the target is not only to increase the frequency response dynamics, but also to reduce the wear and tear of the turbine.

In general, run-of-river power plants with double-regulated Kaplan turbines encounter a high impact when providing FCR. The challenges of permanent blade movements in stand-alone Kaplan units due to FCR provision was analyzed in [18–20]. The drawback is a significant increase in load stress, which reduces the lifetime of the turbines and increases the probability of outages. The author describes that the main driver of providing FCR with run-of-river units is to free up more flexible storage power plants to deliver products with a higher revenue (e.g., frequency restoration reserve—FRR). The outcomes of this analysis were then used to derive specifications for a new turbine design for a turbine replacement.

In [21], an optimal control strategy to provide FCR with hydropower units was discussed. The purpose of the control strategy is to use fast storage power plants for small frequency deviations, while for larger frequency disturbances, RoR on the Danube River are activated.

In [2], benefits of operating a hybrid power plant are listed:

- Ensuring that the BESS is charged with clean energy.
- Allowing the producer to extract value out of the minimum flows.
- Increasing the provision of ancillary services through the large increase in capacity.

On the other hand, a review of the BESS aging caused by FCR provision, based on operational data, carried out in [22] shows that after 5 years of operation, lithium-ion batteries suffered only a loss of 5% in state-of-health (SoH).

In [23], results of different types of aging tests performed by the Italian transmission system operator (Terna) applied to several electrochemical technologies are presented. While some lithium-based technologies were not influenced by the cycle type and by its features in terms of both energy and power, other technologies suffered a 20% capacity decrease after the performed tests. The authors conclude that further research is necessary in order to deeply understand what determines the premature aging of some storage technologies during FCR provision.

For all demonstrators in the XFLEX HYDRO project, an aggregated ancillary services matrix was developed. Within this ancillary services matrix, the performance of each demonstrated technology for different grid services was evaluated [24].

The paper is organized as follows. In Section 2, the demonstrator is explained in detail. In Section 3, the control strategy, monitoring concept and methodology of benchmarking the benefits of the hybridization are described. In Section 4, field results of the demonstrator are presented. A conclusion and outlook are given in Section 5.

2. Description of the XFLEX HYDRO Vogelgrun Demonstrator

In this section, the XFLEX HYDRO Vogelgrun demonstrator is described.

In the run-of-river (RoR) HPP Vogelgrun, four Kaplan units with a nominal power of 35 MW are installed. At this demonstrator, the hybridization of one turbine-generator-unit (TG-unit) with a battery energy storage system (BESS) of 650 kW/370 kWh is assessed. The technical and economical constraints in the optimization of the BESS size were described in [25]. The target of the demonstrator is to improve FCR provision and dynamics with a hybrid system, increase the flexibility capability and, at the same time, reduce wear and tear compared to a non-hybrid TG-unit by 90%. Furthermore, a minimally sized BESS shall be used. The four TG-units provide 4 MW of FCR each. Additionally, the existing speed governor of the hybridized TG-unit shall not be replaced.

In the case of the Vogelgrun demonstrator, the response time of 30 s for FCR provision is met thanks to a hybrid controller and a dedicated algorithm splitting the active power setpoint to the BESS and the TG-unit, which has a slower response.

In Figure 2, the scheme of the control of the hybrid system is shown. A hybrid controller measures the grid frequency and distributes the FCR setpoint to the existing speed governor and the BESS, while considering the state of charge (SoC).
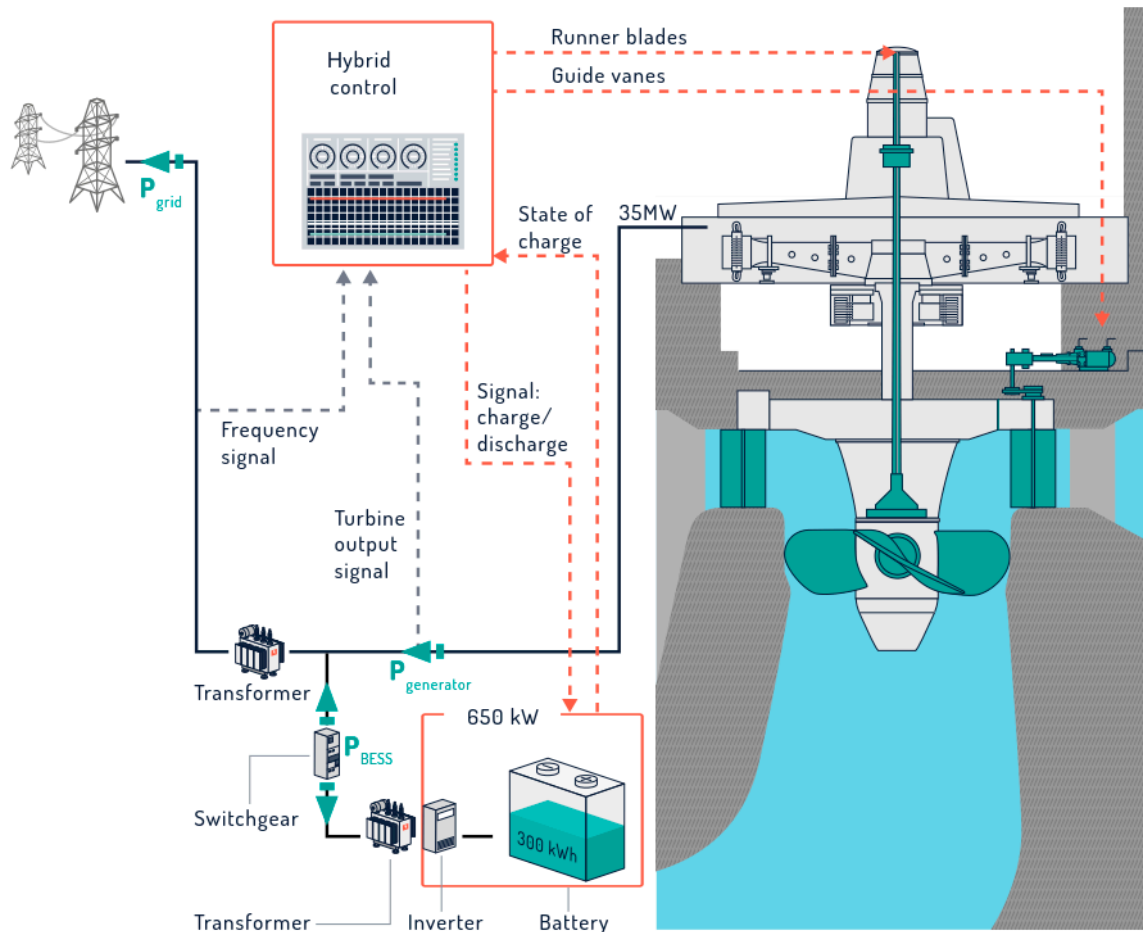

Figure 2. Overview of the hybrid unit setup.

3. Methodology

In this section, the control strategy of the hybrid system is described. Further, the monitoring concept, wear and tear assessment as well as developed real-time simulation models are explained.

3.1. Control Strategy of the Hybridized Unit

The Vogelgrun hybrid demonstrator is driven by FCR dynamic response and by wear and tear reduction. These two goals led to the hybridization algorithm, which consists of controlling HPP and BESS power simultaneously. Indeed, at every moment, the sum of these two powers on the grid has to be equal to the power expected by the TSO regarding the frequency deviation.

The diagram in Figure 3, presents the control overview where grid frequency and BESS SoC signals are the inputs of the algorithm and where BESS power and HPP frequency set points are the outputs of the controller. In general, the HPP's controller uses the frequency signal to modulate its power generation regarding frequency deviation. The aim of the hybridization algorithm is to control the HPP's power through its actual governor, thus utilizing existing hardware. For this purpose, the hybrid controller recreates an

analogic frequency signal to control the existing turbine governor. Computation steps of this algorithm are explained in the following paragraphs.
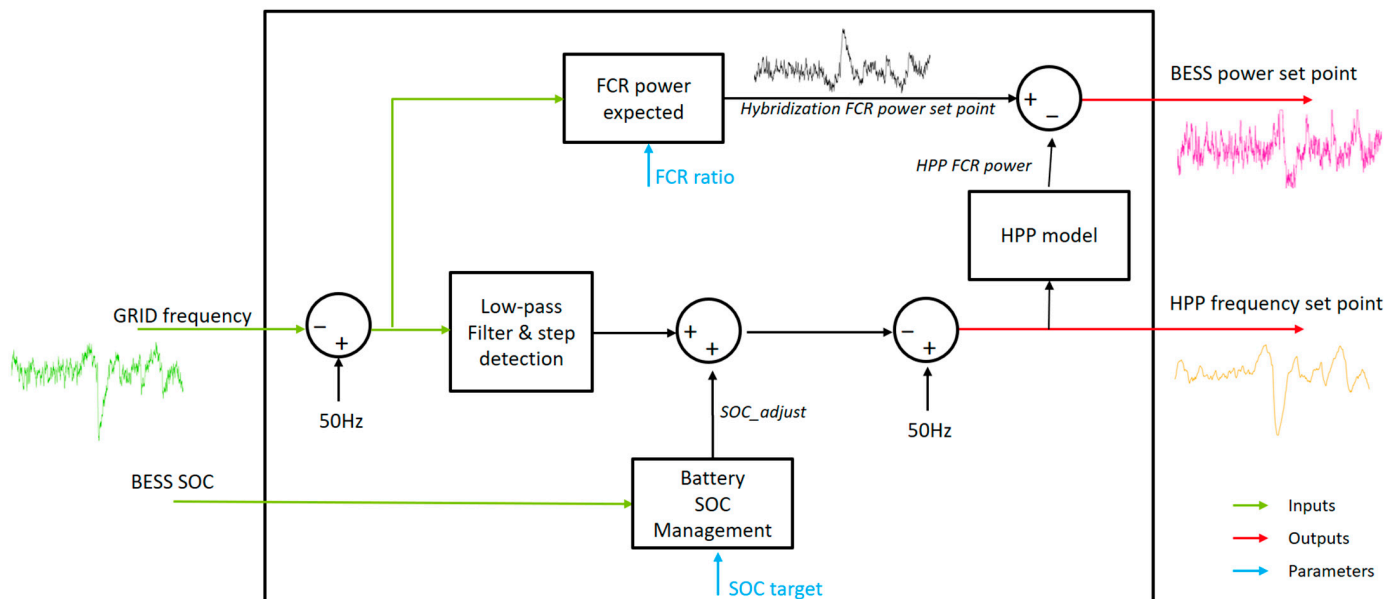
Figure 3. Control algorithm overview.

HPP control is based on filtered grid frequency modulated with SoC management. The first block named "Low-pass Filter & step detection" is a first-order low pass filter and creates the "smooth version" of the grid frequency signal. The time constant of this filter is set to 30 s (modified to 100 s) and was chosen to optimize wear and tear and FCR coverage. Moreover, a step detection process is also computed in this block and compares the temporal variation in the frequency to a threshold. Abrupt variations in the frequency are detected, and the magnitude of filtered signal is boosted by a gain of 1.2 to speed up the power time response of the HPP. Finally, the filtered signal is updated using the signal provided by the block named "battery SOC management". Indeed, when the DC power profile applied to the battery is not symmetrical in terms of energy, efficiency is not 100% and the BESS quickly reaches lower values of SoC. The battery SoC management block addresses this behavior and operates the BESS around a SoC target. The strategy is to modulate energy provided by the HPP to charge or discharge batteries to maintain the BESS' SoC target level.

When the operating SoC does not reach the SoC target parameter, the signal "SOC_adjust" deviates from the frequency set point of the HPP according to the lookup table presented in Figure 4. The input is the delta SoC, computed as the difference between the battery's SoC and a constant parameter SOCtarget (fixed to 0.6, in order to limit battery aging). Therefore, when the SoC is in the range from 40% to 80% (and delta SoC in the range [± 0.2]), the "SOC adjust signal" remains close to 0 and no extra or deficient power from the HPP is used to manage the BESS energy stock. However, when the SoC is in the range from 10% to 40% (and delta SoC in the range [-0.5–0.2]), linear correction is used, and the frequency signal sent to the HPP is decreased. Accordingly, the HPP's power increases and the overproduction is used to charge batteries. The frequency adjustment signal is saturated to $+/-32.5$ mHz and corresponds to the maximum BESS power (650 kVA). In the same manner as presented previously, when the SoC is in the range from 80% to 85% (and delta SoC in the range [0.2–0.25]), linear correction is used, and the frequency signal sent to the HPP is increased. As a result, the HPP's power decreases and the BESS is discharged to provide more energy to the grid.
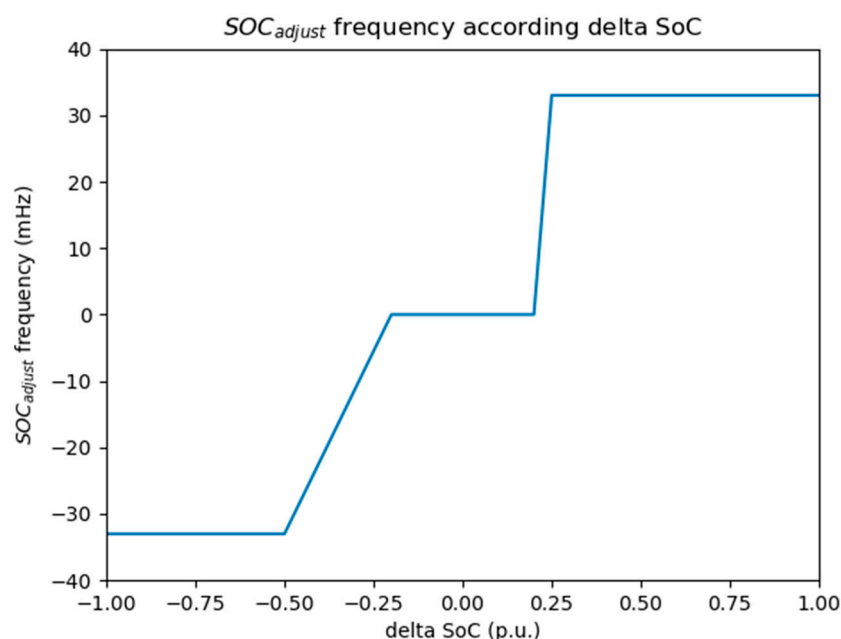
Figure 4. Frequency adjustment algorithm.

The BESS power setpoint is the difference between the power required by FCR response ("Hybridization FCR power setpoint") and the power provided by the HPP controlled with frequency signals from a hybrid controller. The regulating power, "Hybridization FCR power setpoint", is computed as the frequency deviation from 50 Hz multiplied by a ratio, "FCR ratio", fixed to 20 MW/Hz. Unfortunately, the power provided by the HPP controlled with frequency signals from a hybrid controller is physically unmeasurable. This signal is estimated by the "HPP model" block from the HPP frequency setpoint, and it corresponds to a first-order model with a time constant measured on the TG-unit.

Considering the rules of the SoC management block described previously, Figure 5 presents the behavior of the controller regarding the SoC (blue curve in the middle plot) during a frequency deviation (red curve in the top plot). In the case of under-frequency (<50 Hz), the battery is discharged, and the SoC signal decreases (from time 250 s to 580 s). After time 300 s, the SoC is lower than 40% and the SoC management strategy influence is visible with the difference between the HPP frequency signal setpoint with adjustment (green curve in the top plot) and without adjustment (output filter signal, purple curve in the top plot). After time 580 s, the BESS's output power (pink curve in the bottom plot) becomes negative, and the BESS is charged with increased HPP output power (green curve in bottom plot).

Additionally, an aging campaign on a testing bench with climatic chamber regulation at 25 °C on lithium-ion C/NMC cells representative of the ones used in the Vogelgrun demonstrator was conducted. The power profile is made of 2 phases, and it was tested in February 2020. The aging phase consists of applying 3 weeks of the current profile based on a February 2018 FCR power profile followed by a check-up test phase to the control cell's capacity. The initial state of health (SoH) is not at 100% as experimental cells faced calendar aging prior to the aging campaign. Figure 6 shows the comparison between experimental (in red) and model prognostic results (in blue). This comparison highlights that the model prognostic is very close to the experimental results and the SoH error, defined as total energy throughput divided by 2-times the nominal energy, remains below 1% after 1200 equivalent cycles.

In [26], a model-based control strategy for optimal asset management of hydroelectric units in run-of-river hydropower plants is presented. The proposed control strategy aims to operate the unit at the best efficiency while improving water flow management and minimizing components' wear during frequency containment reserve provision.
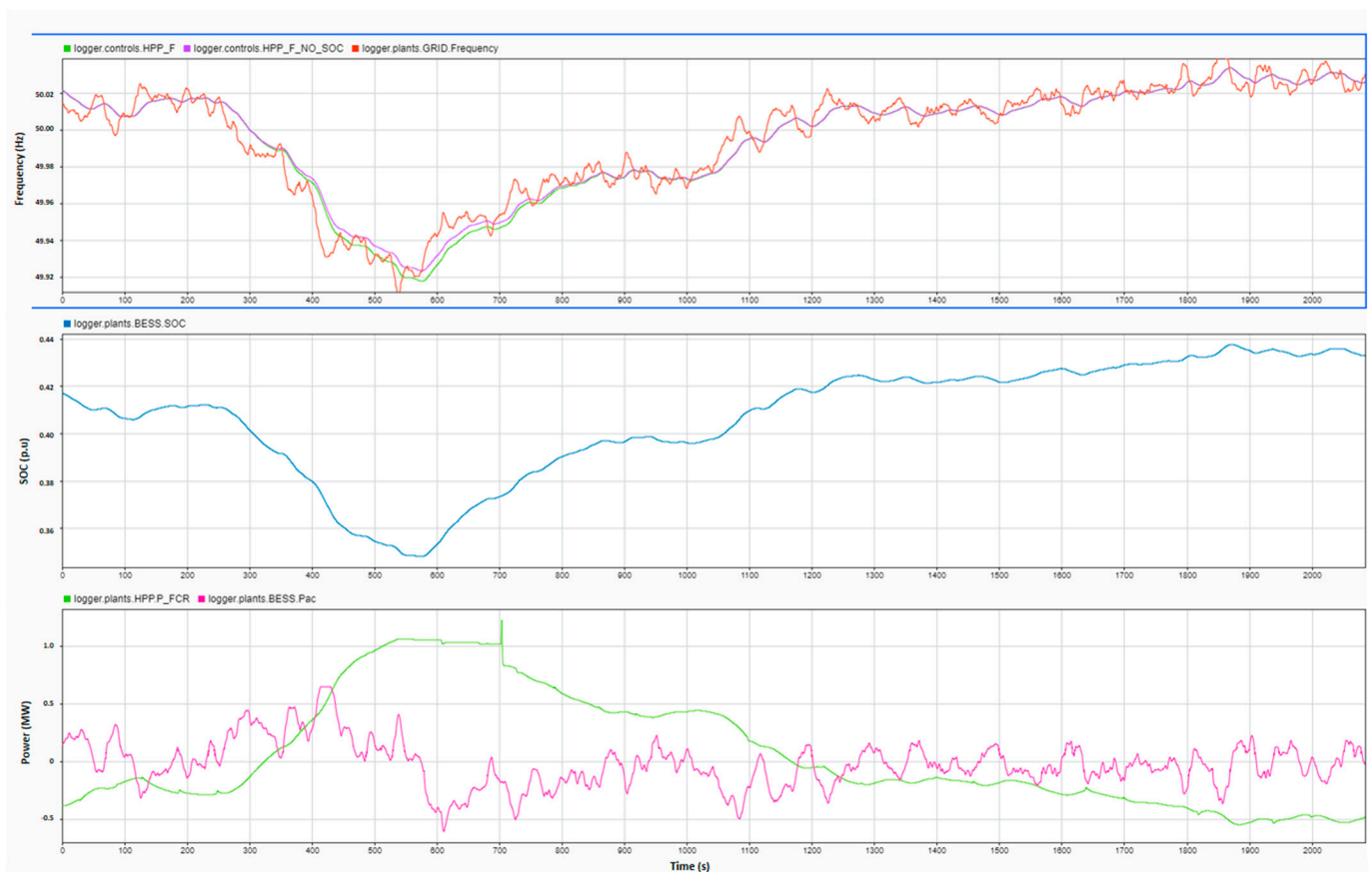
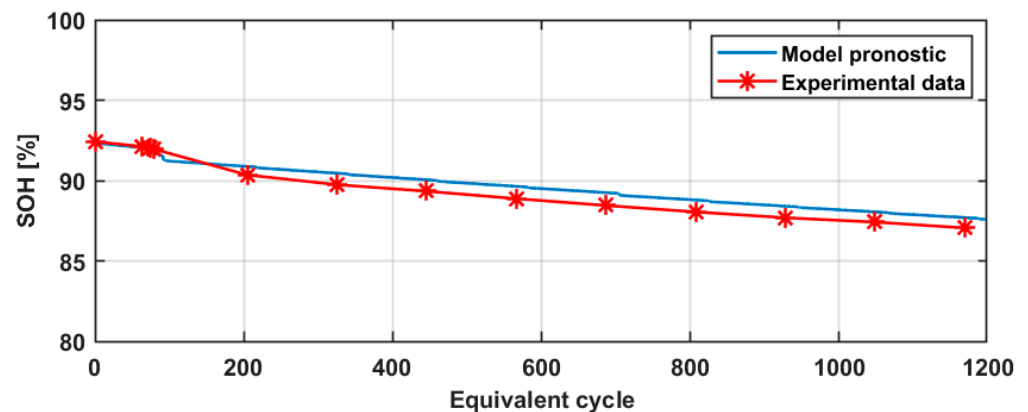**Figure 5.** Simulation of BESS operation with SoC management implementation.

Figure 6. Experimental results vs. model prognostic comparison.

3.2. Monitoring Concept

In Figure 7, the overall monitoring concept is depicted. There are four systems deployed either via Modbus TCP/IP or analogue signals (voltage signals) connected to each other. The blue circle marks the HIPASE hybrid controller system, including the BESS and the SCADA monitoring system running on an industry PC. Due to security reasons, there is no access to the hybrid controller via a VPN. To exchange signals with the MVX monitoring systems, analogue signals are used. From the MVX, the collected measurement signals from unit 1 and unit 3 as well as selected signals from the hybrid system are distributed to the Hydro-Clone and Metris DiOMera. Each of these three systems is remotely accessible.
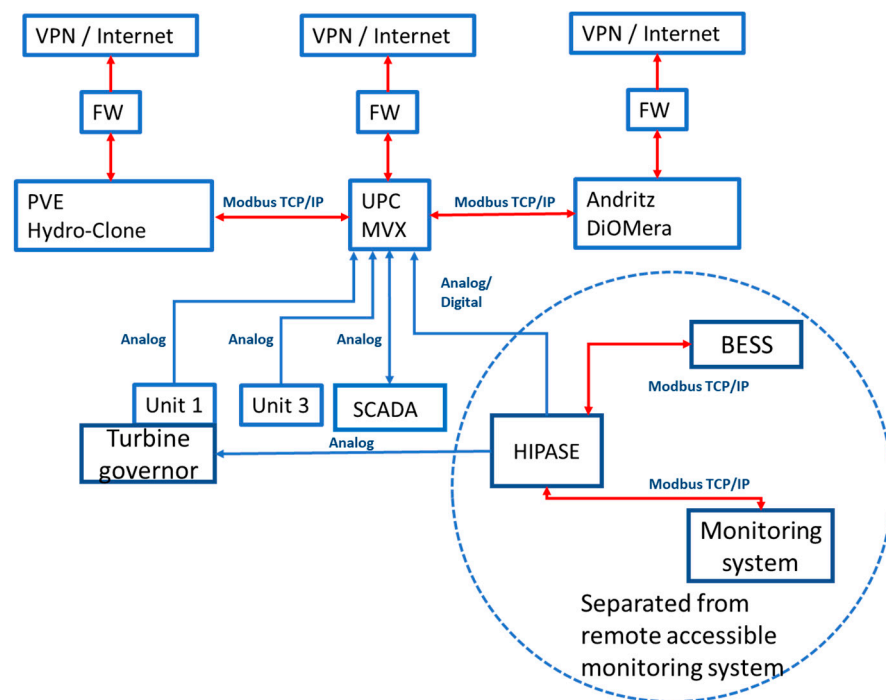
Figure 7. Overview of monitoring concept.

3.3. Wear and Tear Assessment

The mainly affected mechanical components of a Kaplan turbine during primary regulation in the sense of wear and tear are the turbine runner and the guide vane mechanisms. These parts were modelled in 3D and analyzed with finite element methods (FEMs). The needed hydraulic loads acting on runner blades and guide vanes were obtained from separate computational fluid dynamics (CFD) simulations (Figure 8). Frequent adjustments of the runner blade and guide vane angular positions primarily induce fatigue-related damaging impacts during FCR provision. At each adjustment cycle, friction encountered when moving blades and vanes back and forth must be overcome, leading to certain stress amplitudes at the parts. Wear depending on the turning distance of the trunnions in the bearings and the bearing load is calculated with the pressure distributions gained from the finite element analyses (Figure 9). The FE models are simplified using cyclic symmetry but contain the full mechanism.
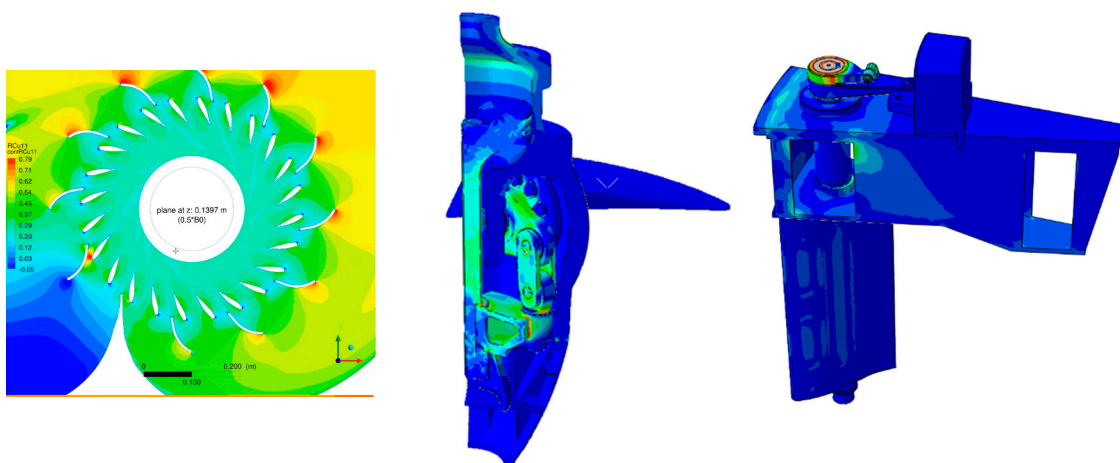

Figure 8. Flow condition at the guide vanes (**left**); Stress amplitude results at runner and guide vane mechanism finite element model (**middle** and **right**).
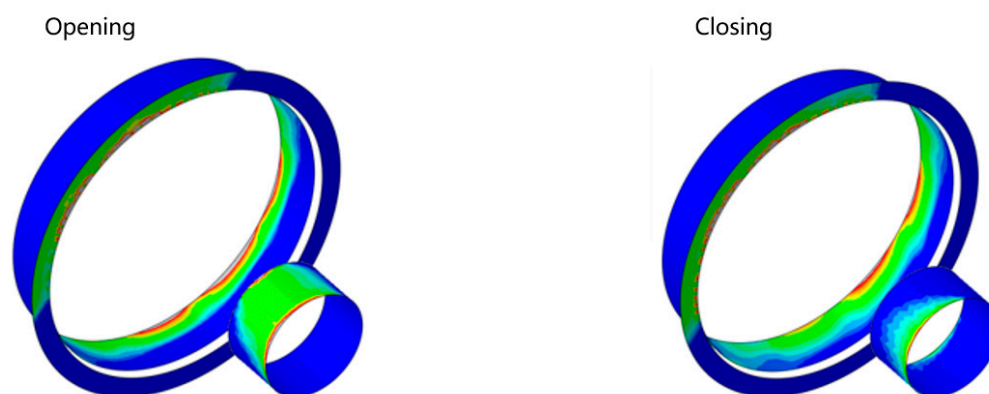
Opening   Closing

Figure 9. Contact pressure distribution at runner blade bearings: opening (**left**), closing (**right**).

Hill charts for wear (bearing deterioration) and fatigue (utilization of the turbine parts) should describe the damage in each point of operation for the runner and the guide vane mechanisms. In Figure 10, the utilization of approximately one year of primary regulation is presented. The link pin at the runner is the most endangered part regarding fatigue failure. With the fatigue hill chart points, the operation with high and low utilization can be detected.

Metris DiOMera, the digital solution by Andritz Hydro for predictive maintenance, was installed in Vogelgrun on a computer in the powerhouse. In Metris DiOMera, health and trend indicators are defined that describe the current state of a component, or group of components in the units, and that predict its future behavior. It is distinguished from the so-called key diagnostic indicators (KDIs) that evaluate the past and present condition of a component and key trend indicators (KTIs) that predict future evolution of the KDIs. KDIs are normalized, where 0% means good condition and 100% means critical condition. For Vogelgrun, the main emphasis is put on KDIs that analyze wear and tear of the turbine with the aim of quantifying the improvement in the hybrid mode on the turbine aging. Wear of runner blade bearings and fatigue of the runner regulating mechanism were identified as the most relevant indicators.

The status of wear of runner blade bearings: Wear of the runner blade bearings depends on the distance that is covered by the movement of the runner blades (the so-called mileage), the contact pressure and a wear coefficient. The mileage is computed from the acquired runner servomotor position, the contact pressure comes from FEMs, and the wear coefficient is chosen according to the literature. Wear in [mm] is converted into a non-dimensional KDI by defining a critical limit value for wear.

The status of fatigue of the runner regulating mechanism: From the recorded servomotor's opening and closing pressures, a servomotor force is computed that is then converted into stress by applying FEM results. The number of load cycles is determined using rain flow counting. Using Miner's rule and an appropriate S–N curve yields cumulated damage for the considered period. The same method can be applied to different parts of the runner regulating mechanism.

In order to compute these indicators based on real operation, operation data are acquired from the MVX monitoring system for unit 1 and unit 3. Therefore, the data of unit 3 serves as comparison to the hybrid unit 1.

Metris DiOMera comes with a web-based graphical user interface (GUI) showing data visualization of all acquired and computed signals as well as the health and trend indicators. In Figure 11, one tab of the GUI showing histograms of acquired active power of the turbine and head is depicted, as one example. The plot shows the distribution of the operating points and durations. One can observe that the unit was operated mainly between 15 MW and 25 MW during the selected period. In the dispatch of the unit, the water levels are considered to maintain those on the Rhine River for shipping traffic. A discharge setpoint for each 15 min interval is received for the power plant.
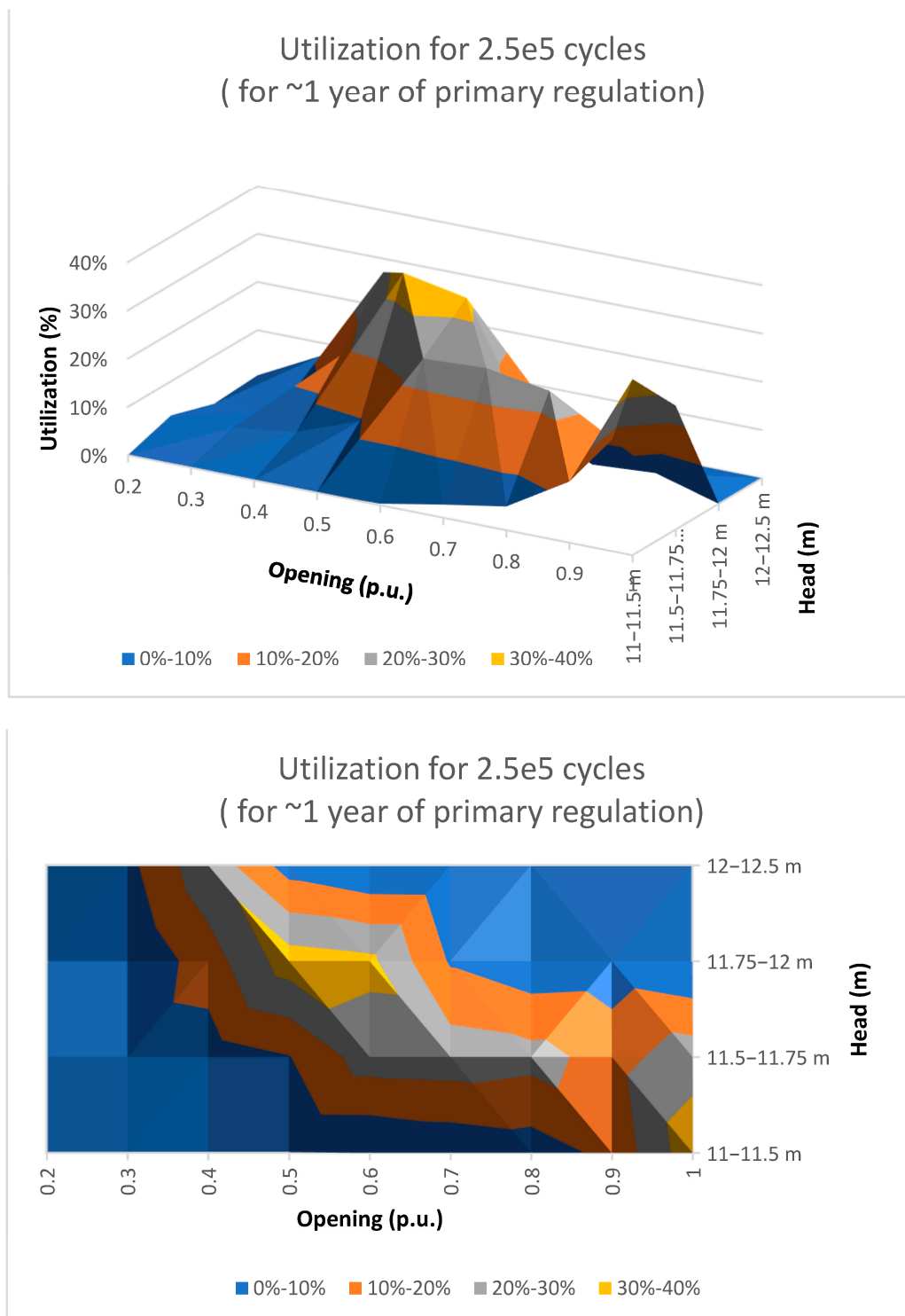
Figure 10. Utilization for approximately 1 year of primary regulation.

3.4. Real-Time Simulation Models

A SIMSEN model of the Vogelgrun HPP was developed including the water intake, the Kaplan turbine and the draft tube of the unit (Figure 12). Particular attention has been paid to the modeling of the spiral case in order to consider the evolution of the cross-sectional area and the distribution of the discharge. The hydraulic part of the numerical model was validated by comparing the simulation results with a time series of static pressure in the spiral case and the rotational speed of the Kaplan turbine measured during an emergency

shutdown performed in 2015 [27]. The SIMSEN model also includes a turbine governor combining the control of the flow of the Rhine River and the FCR control. The turbine governor is operated in the guide vane position control mode and uses an on-cam lookup table to define the blade angle setpoint as a function of the head and the guide vane position. The validation of the control part in the SIMSEN model was performed by comparing the numerical simulation results with the site measurements performed over 2 days in April 2021, as seen in Figure 13.
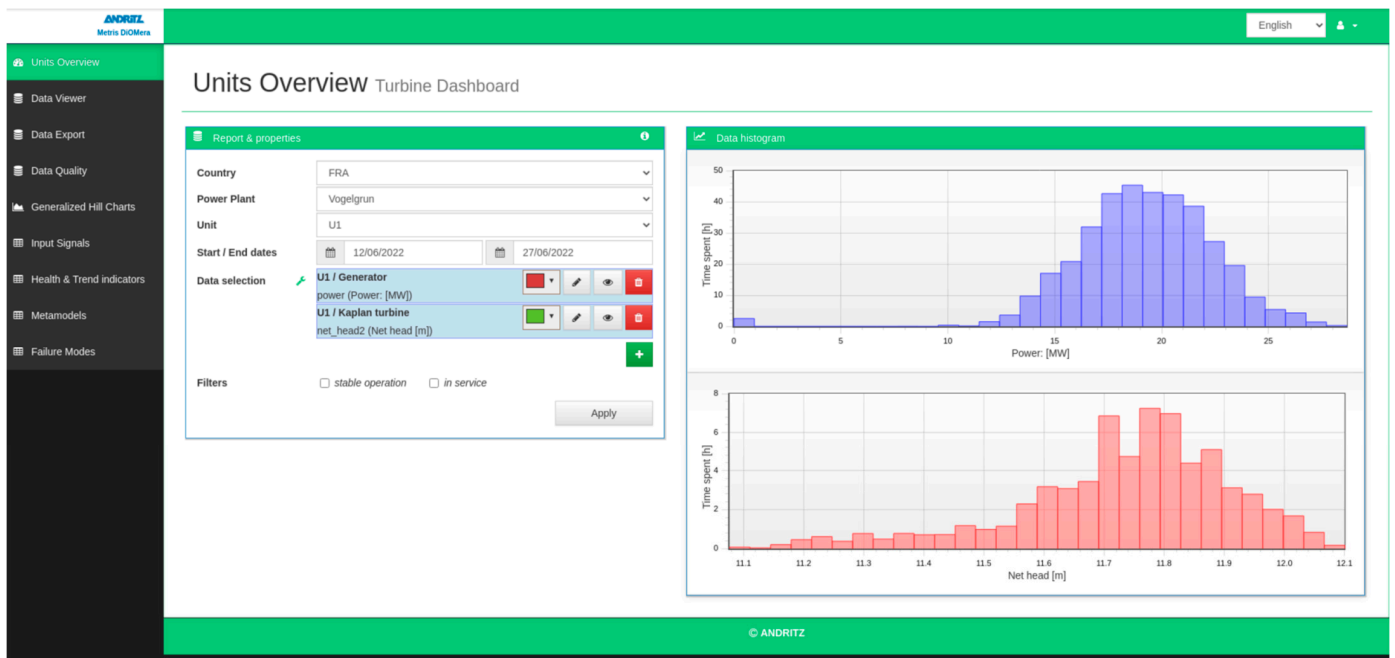
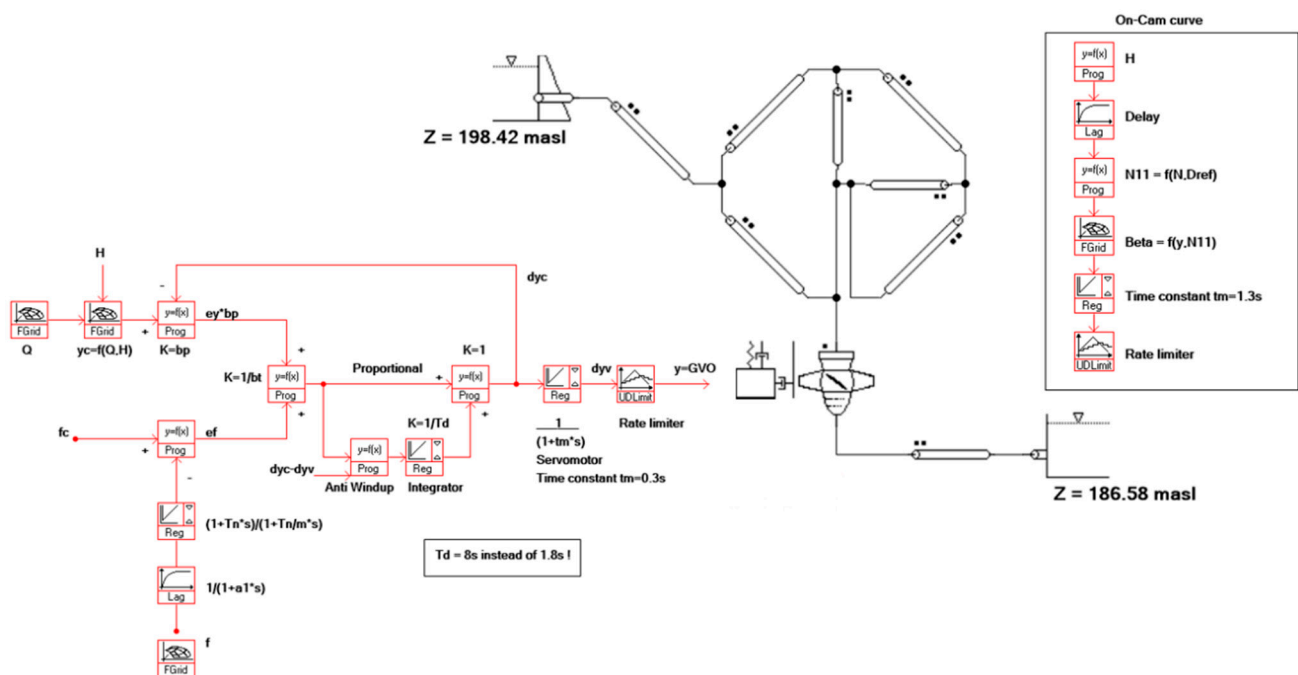**Figure 11.** Screenshot of the graphical user interface of Metris DiOMera in Vogelgrun.

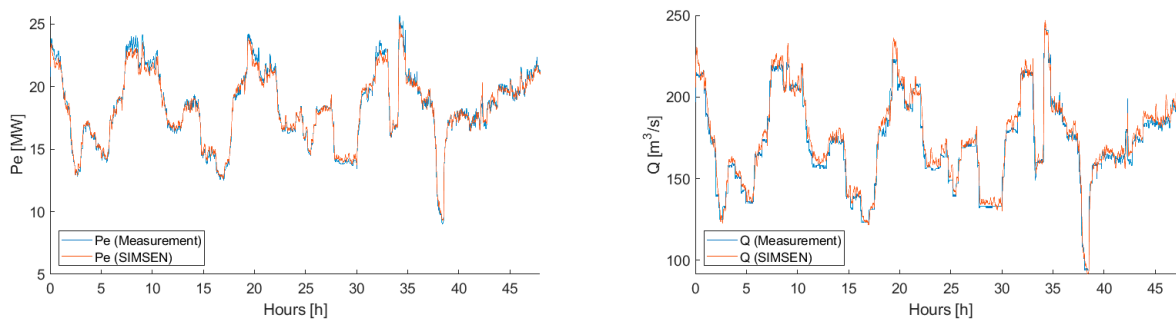**Figure 12.** SIMSEN model of the Vogelgrun HPP.

Figure 13. Comparison of power and discharge measurements (blue line) made over 2 days in April 2021 and numerical results (red line).

By using turbine flow setpoint and grid frequency time histories, it was possible to reproduce the time evolution of the active power, guide vane opening and blade angle with good agreement. Thus, the good reproduction of the active power Pe validated the characteristic curve of the Kaplan turbine. Moreover, the good agreement for the guide vane opening confirmed the turbine governor's behavior. Finally, the on-cam curve also attested to the comparison of the blade angle beta. This model was then used for real-time monitoring of the Vogelgrun HPP with Hydro-Clone.

Hydro-Clone is an innovative real-time simulation monitoring system (RTSM) based on a well-calibrated and validated SIMSEN model of the hydropower plant capable of reproducing in real time any dynamic behavior of the plant based on the boundary conditions measured in situ, i.e., it is a digital twin [28–30]. This system allows continuous diagnosis of the health of a hydropower plant with digital cloning of the main hydraulic and electrical components of the plant. The Hydro-Clone's general concept is illustrated in Figure 14. The system manages the tasks of real-time acquisition and transfer of boundary conditions and measured quantities to the SIMSEN model, as well as data processing and diagnosis of the HPP health status. A custom-built archival storage system and an associated database allow for the display and analysis of previous results. The analysis and comparison of simulated and measured quantities enable us to understand, at any time, the fitness and behavior of all essential components of the system and to estimate non-measured/non-measurable quantities throughout the entire system.

The immediate benefit of this digitalization is that it allows the non-measured/non-measurable quantities to be monitored at any time without the physical installation of additional sensors. In the case of the Vogelgrun HPP, it was decided to take advantage of this type of digitization to evaluate the impact of the BESS on the movements of the guide vanes opening (GVO) and the runner blade opening (RBO) by adding three additional real-time models operating in parallel in the Hydro-Clone. The characteristics and goal of each model are summarized in Figure 15. The clone model #1 is the classic monitoring, which replicates the behavior of the real unit by imposing the measured guide vane openings and blade pitch angle in the simulation. The clone model #2 includes the turbine governor model, with the guide vane opening setpoint and grid frequency as inputs. In this mode, the movement of the guides and blades is therefore a result, as they are driven by the turbine governor. This model enables us to emulate the behavior of unit 1 without the BESS regardless of the mode of operation of the real unit. The clone model #3 follows the same philosophy as the model #2 except that the input is the low pass filtered grid frequency, as computed by the hybrid controller (Figure 3). This allows us to replicate the behavior of the hybridized unit 1 with the same control structure as when the BESS is activated. It was verified that the behaviors of models #2 and #3 correspond to the real unit when the battery is deactivated or activated, respectively. Finally, clone #4 simulates the behavior of the unit when the FCR response is disabled. This enables us to identify the contribution of level regulation to the movement of GVO and RBO. These various versions of the digital twins with the unit controller provide a basis for comparison that allows direct confrontation of the hybrid and non-hybrid modes under the same operating conditions.
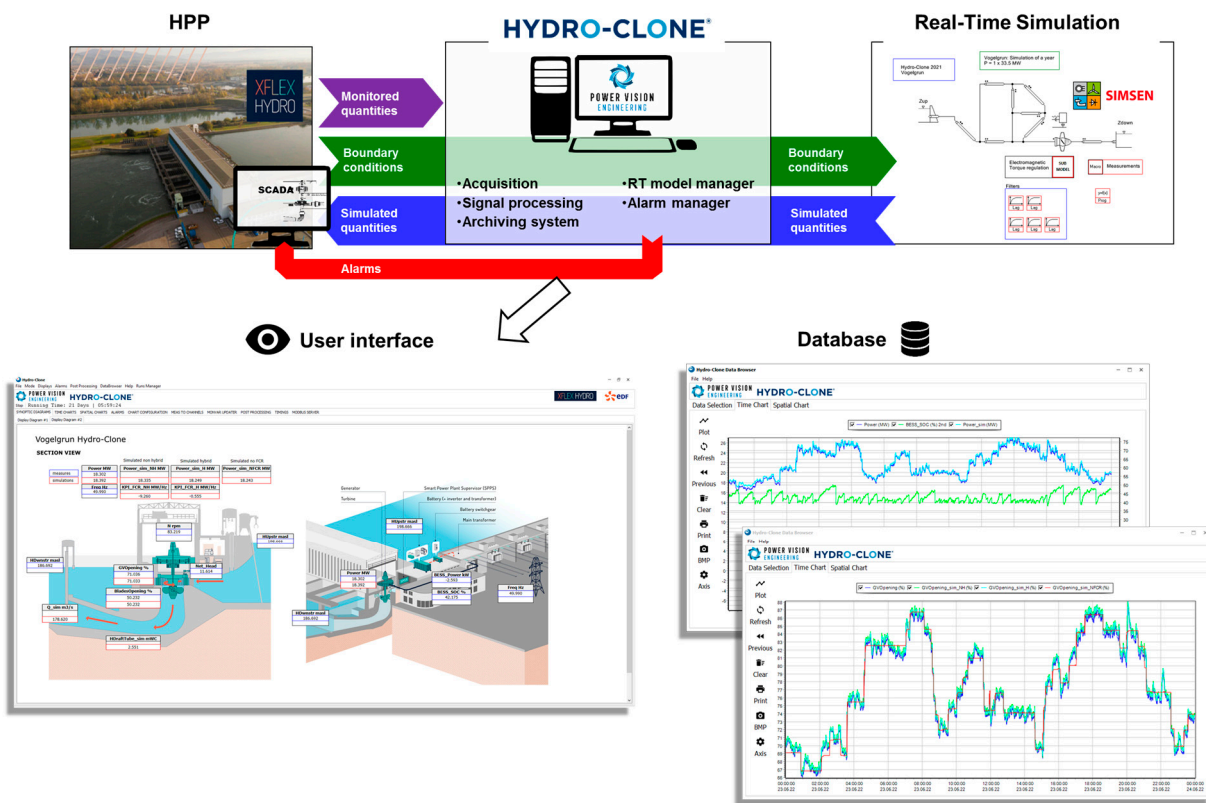
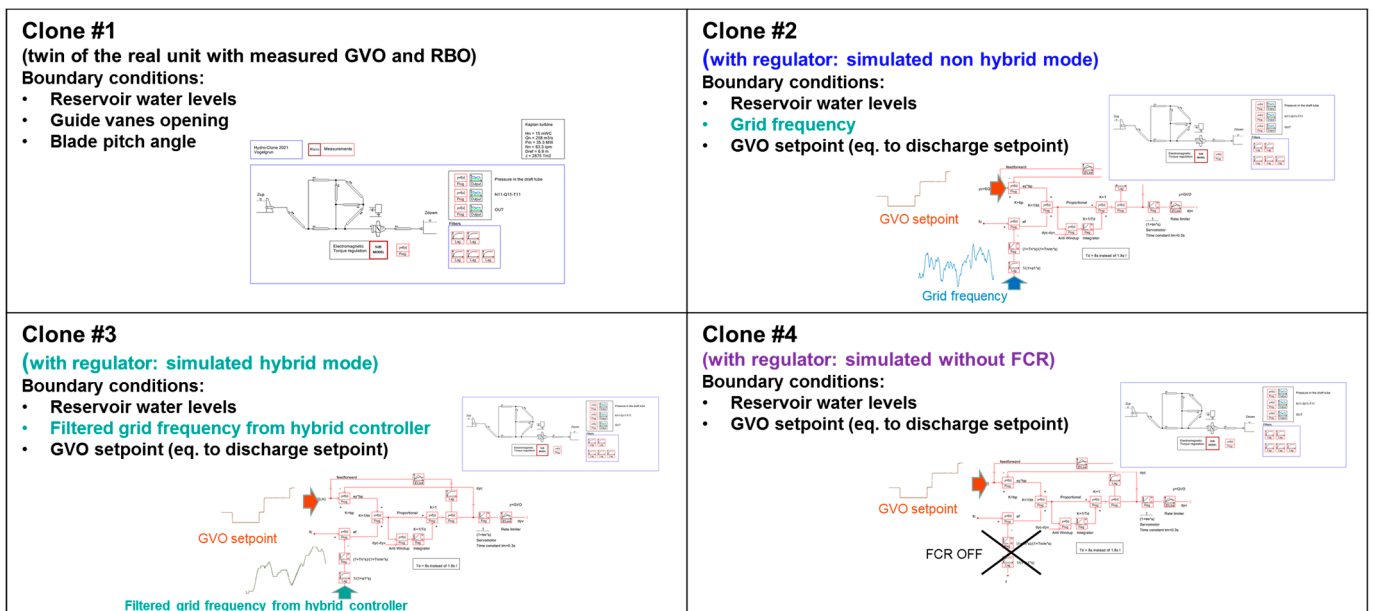**Figure 14.** General concept of Hydro-Clone system based on real-time simulation.

Figure 15. Summary and characteristics of the four real-time models deployed in Hydro-Clone.

4. First Assessment of Hybrid Operation

In this section, the first results of the assessment of hybrid operation are presented. First, the evaluation of the operating scheme is discussed. After that, the wear and tear assessment, with the identification of the most critical element is described. After that, the outcome of real-time models is presented.

4.1. Evaluation of the Operating Scheme

In Figure 16, box plots of the SoC, BESS power and turbine power for one selected week is presented. Each box plot shows the 1st, 10th, 50th (horizontal line in the rectangle), 90th and 99th percentiles. The red dot indicates the mean value of the sample. On the upper left figure, the BESS active power is plotted. Overall, 98% of the values were ±500 kW during that week. Overall, 50% of the setpoints were within ±200 kW. Hence, for half of the time, the BESS was only loaded with nearly one-third of its rated power. The upper right box plot shows the distribution of the SoC for the same week. The SoC is maintained close to 42.5% (mean value—red dot). Only on the 19th of May, does the 99th percentile exceed 50% SoC. Due to the SoC management, about 10% of the values are below 40% SoC. On the lower right plot, the distribution of the measurements of the turbine's active power output is presented. On the first three days of the week, the output was higher compared to the rest of the week. Last but not least, on the lower right plot, the box plot of the frequency of the grid is shown.
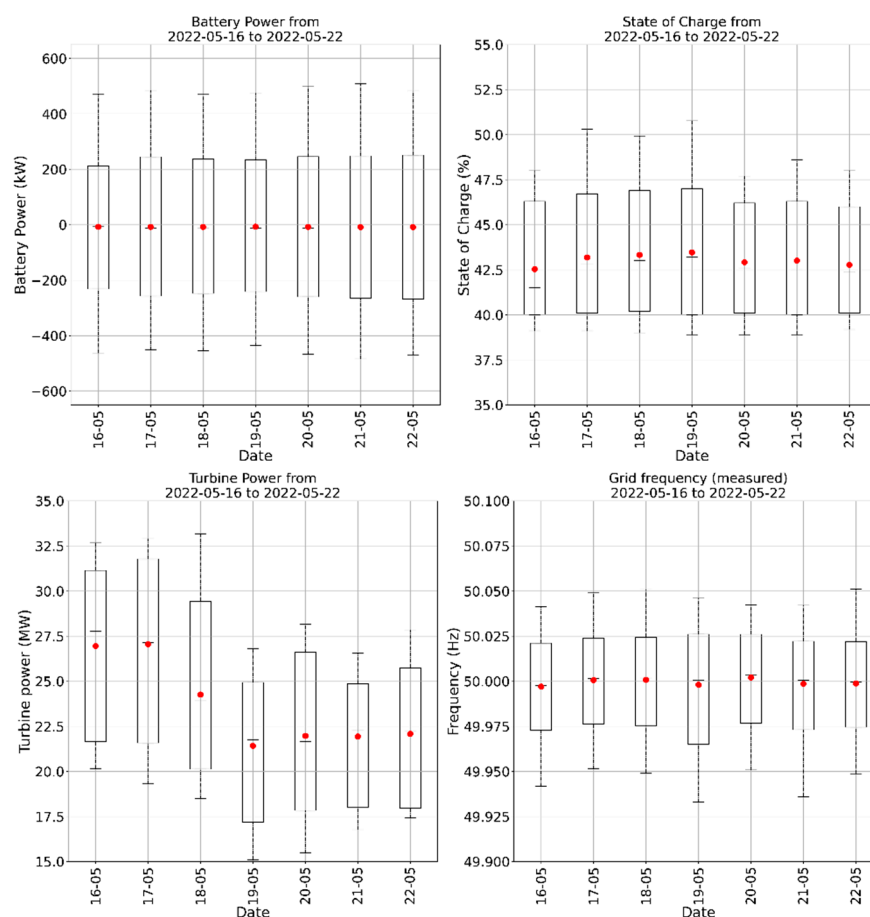

Figure 16. Box plots of the BESS power, SoC, turbine power and grid frequency for one selected week. Box plots showing 1st, 10th, 50th (horizontal line in the rectangle), 90th and 99th percentiles. Red dots indicate the mean value of the sample.

Figure 17 shows the box plot for two frequency signals. On the left side, the measured grid frequency is plotted. The FCR response of the hybrid system is calculated based on this signal. The response is split to the turbine and the BESS (Figure 3). Thereby, the speed governor of the TG-unit receives an emulated frequency signal (Figure 17 right). One can note that the percentiles of the emulated signals are closer to the nominal frequency than the measured grid frequency. In consequence, the wear and tear of the TG-unit is reduced.
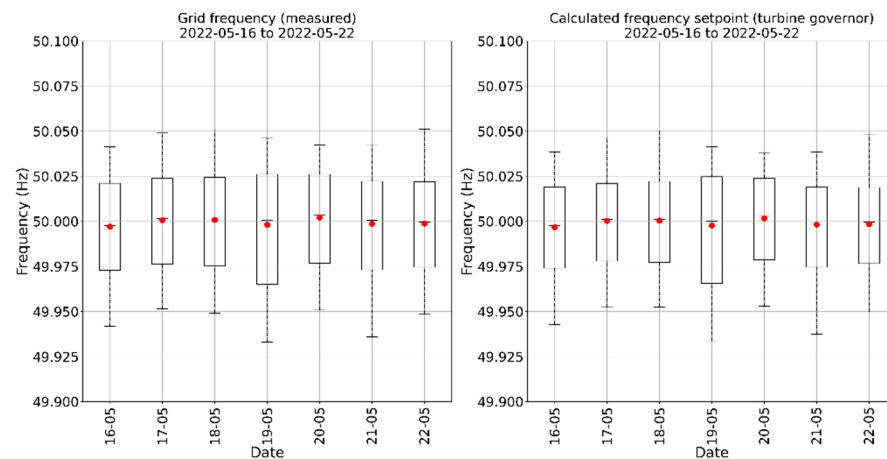
Figure 17. Box plots of the measured and emulated frequency. Box plots showing 1st, 10th, 50th (horizontal line in the rectangle), 90th and 99th percentiles. Red dots indicate the mean value of the sample.

Thanks to empirical battery's aging model, the cell's capacity loss was simulated ([8]). A simulation of the hybrid system over two years, while considering real conditions (water level, flow rate and grid frequency) two times in a row of the year 2018, showed that the battery cell's state of health KPI (SoH) reaches 87%. In other words, the battery loses 13% of its initial capacity after 2 complete years of hybridization operation. After one year of real operation, the SoH calculated with the BESS decreased to 98%. Explanations are that the SoC was kept close to 50%, that the unit was not in hybrid operation at all times and. Furthermore, a pre-defined power profile test with BESS was performed before the start of the hybrid operational phase. The BESS performance for that power profile will be periodically benchmarked. This will be used as a second KPI to evaluate the aging of the BESS.

4.2. Wear and Tear Assessment

The calculated servomotor forces used to actuate the blades were compared with measurements. Discrepancies lead to an adjustment of the measurements.

Even though some of the propeller curves may seem incomplete, the on-cam points could be extracted to create the following comparison between the CFD and prototype, which shows quite a good agreement (Figure 18).

In the FEM simulations of guide vanes and the runner blade mechanism, the most critical component for a failure and an unplanned outage is identified. It is the pin of the link connecting the cross head with the runner blade lever. The components of the guide vane mechanism are not critical. A correlation of the servomotor force and the stress at the pin can be established. The measured servomotor force variations lead to stress amplitudes (Figure 19) and, with the number of load cycles, to utilization of the link pin. This utilization safeguards the reserve against failure. Regarding wear, the most critical component is the radial bearing located at the outer side of the runner trunnion.

The results from the above-mentioned FEM simulations are taken as an input for the two Metris DiOMera indicators that compute wear and material fatigue based on real operation acquired through the monitoring system. As an example, Figure 20 shows the page summarizing the indicator "Wear of runner blade bearing" for unit 1.
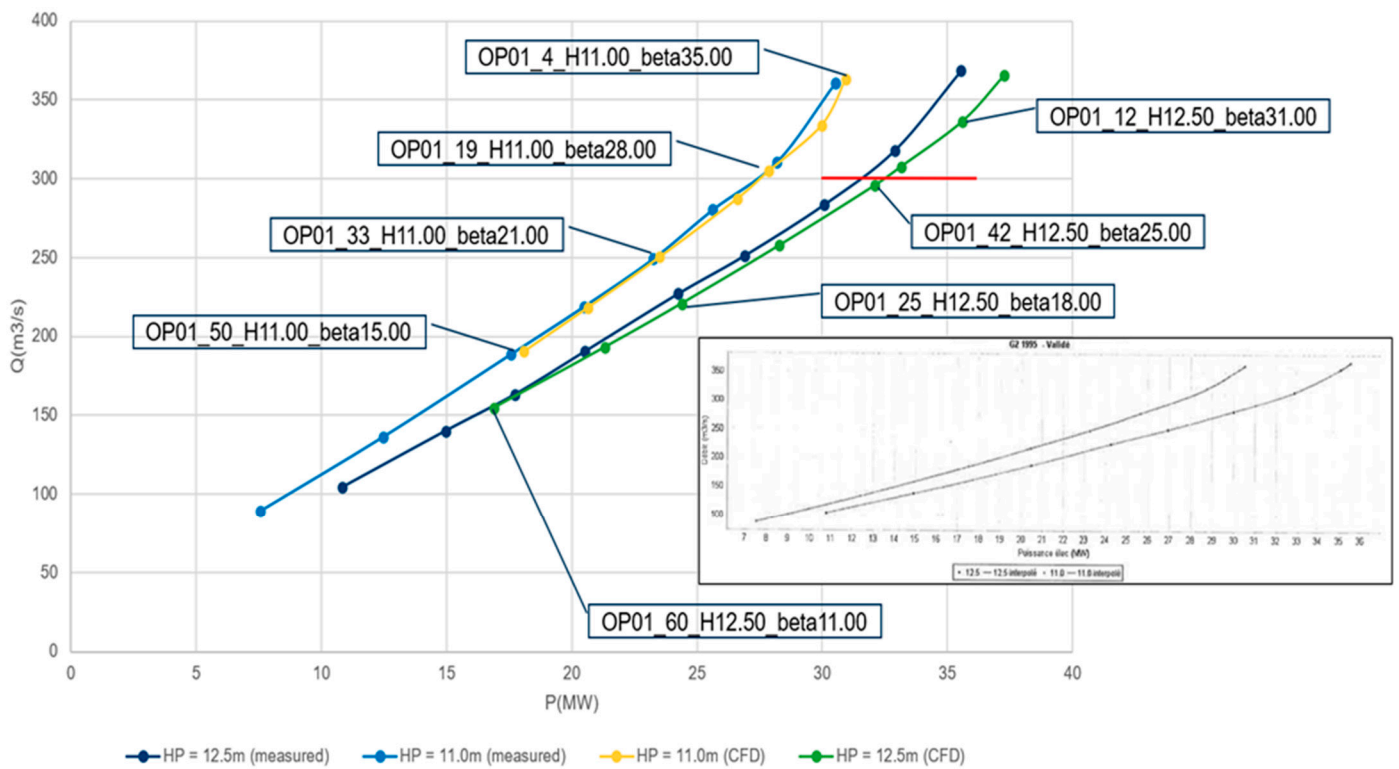
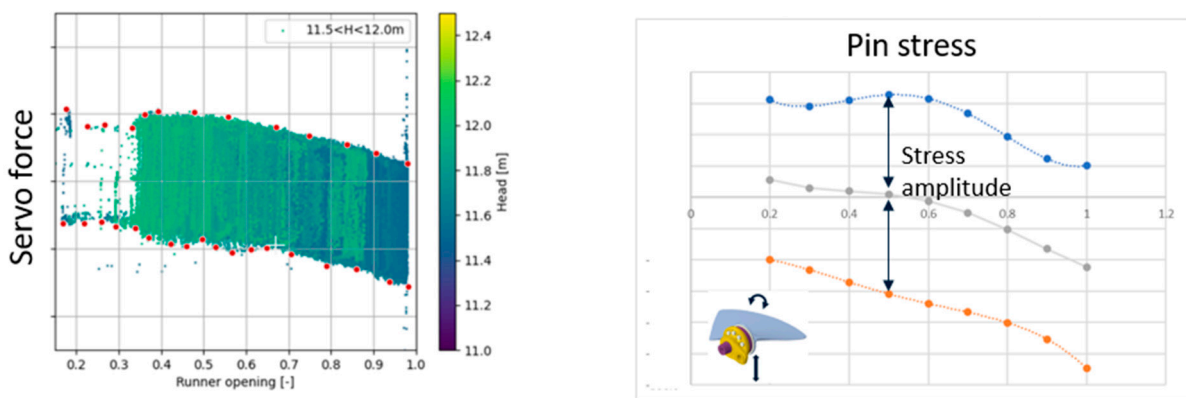**Figure 18.** Comparison between CFD data and prototype data.

Figure 19. Measured servomotor forces and related pin stress.

4.3. Outcome of Real-Time Models

The various declination of the digital twins presented in Section 3.4 make it possible to evaluate the reduction in the mileage of the movements of the guide vane and blade openings that can be attributed to the battery during daily operation. The comparison of the simulated guide vane openings and runner blade openings in hybrid and non-hybrid modes for one day of operation is illustrated in Figure 21. As previously explained, the non-hybrid mode consists of using the grid frequency as the input to the turbine governor, while the hybrid mode uses the "HPP frequency set point" schematized in Figure 3, which corresponds to a low pass filtered version of the grid frequency, to drive the turbine speed governor. Consequently, the hybrid mode reacts to a smoother frequency signal, which results in less movement of the GVO and RBO. As can be seen on the right side of Figure 20, this reduction in movement is easily noticeable but is mostly present for small deviations around the mean value of the GVO and RBO positions.
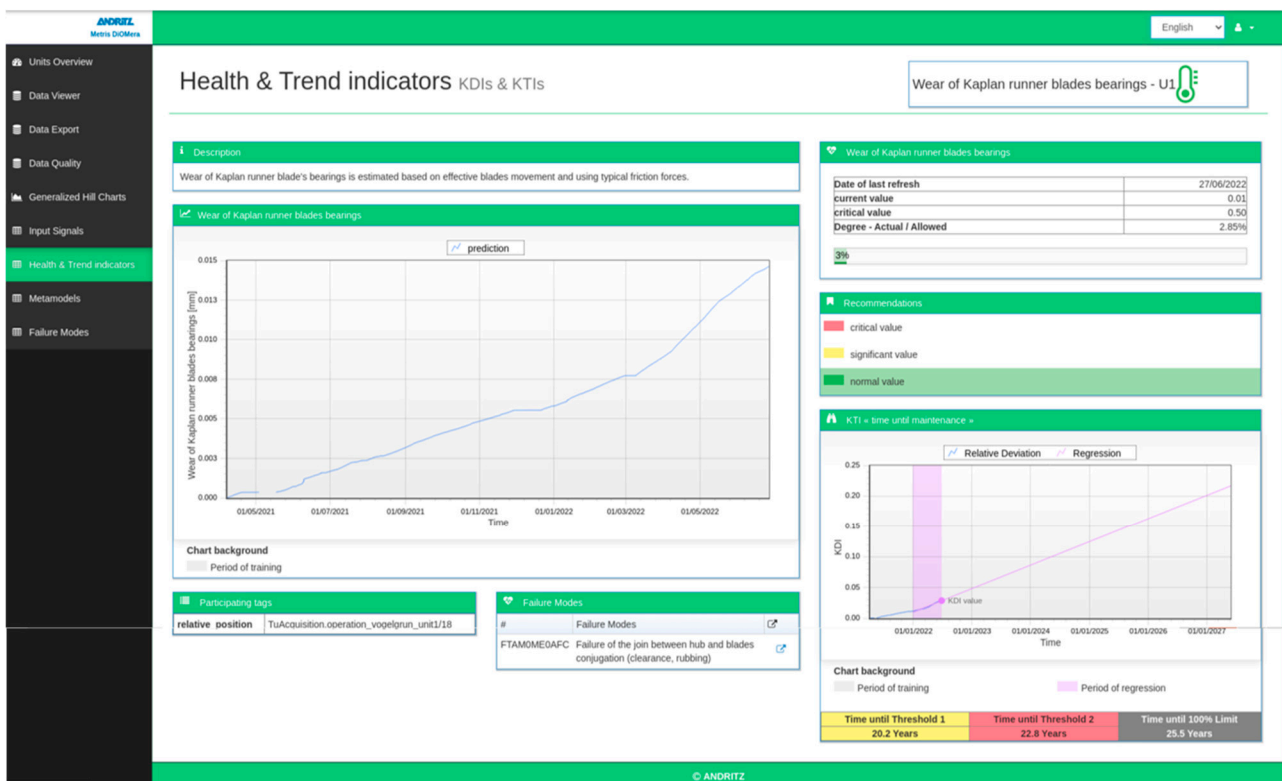
Figure 20. Metris DiOMera page summarizing the wear of runner blade bearing indicator of unit 1.
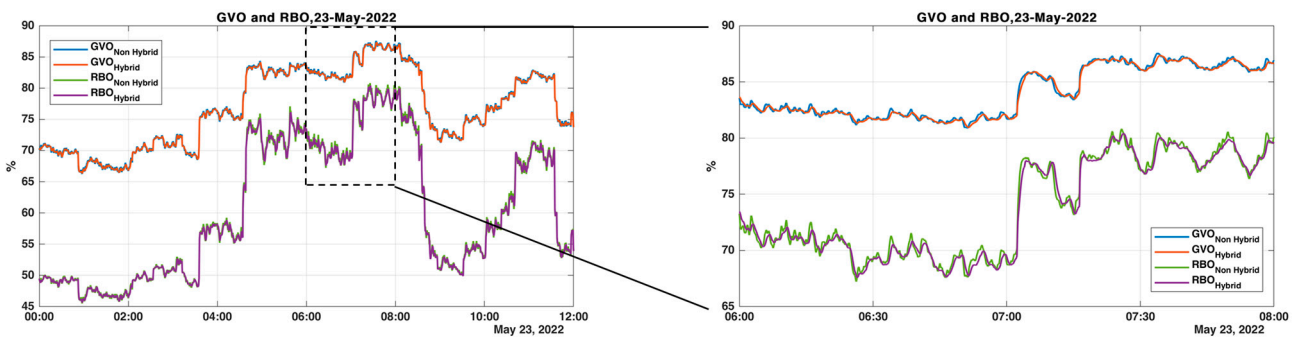

Figure 21. Comparison of the simulated guide vane opening and runner blade opening in hybrid and non-hybrid mode.

To further quantify the benefits of the BESS on reducing the solicitation of control mechanisms, Figure 22 shows the histogram of the GVO and RBO variation during one typical day of operation with the BESS. As it can be observed, the hybrid mode leads to a significant reduction in the number of small-amplitude movements for both GVO and RBO, while the number of large-amplitude motions (>5 mm) is not affected by the presence of the BESS. This is expected since large-amplitude movements are caused by the level control, whereas the BESS is designed to reduce the movement from the FCR provision. Nevertheless, these small movements have a significant impact on the total mileage of the GVO and RBO. In this way, the hybrid mode reduces the total mileage of the guide vanes by 43%, while the runner blade's opening movement is reduced by 40.8%. It is worth noting that the proportion of mileage that comes from level regulation represents 13.5% for GVO and 24.5% for RBO, respectively. The BESS also allows a significant reduction in the number of sign changes in the movement of GVO and RBO. Eliminating small movements reduces the number of panel changes by 67% for guide vane openings and 50.7% for runner

blade openings. This type of result is encouraging to lower the fatigue load of mechanisms by reducing the number of cycles to which they are subjected.
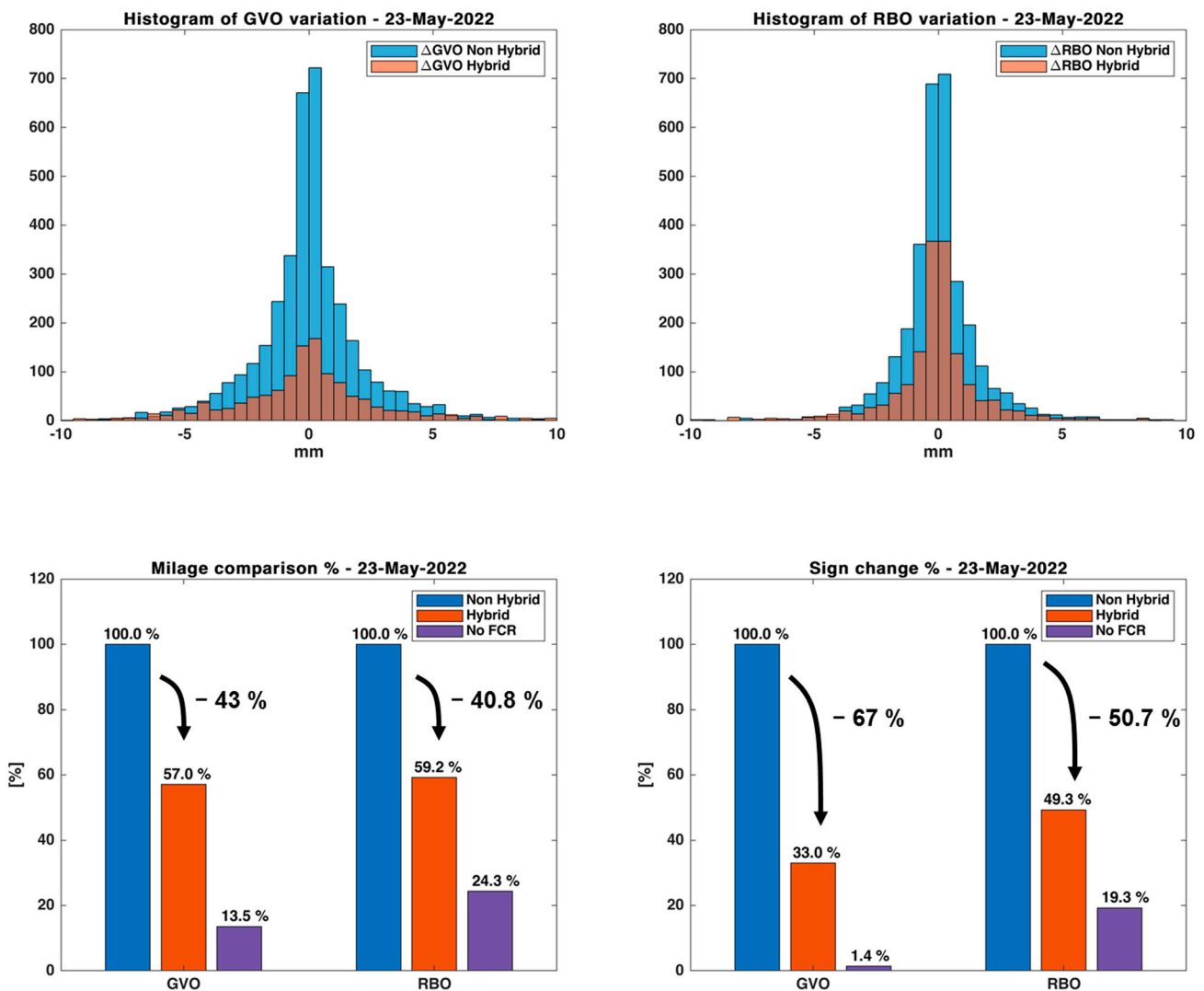

Figure 22. Assessment of the reduction in mileage and number of sign changes for the guide vane opening (GVO), and runner blade opening (RBO), in hybrid mode.

5. Conclusions and Outlook

It was demonstrated that due to the hybridization, the mileage of the guide vanes and runner blades could be reduced. In that regard, the estimated reduction in wear and tear at the beginning of the demonstration matches the achieved reduction very well. With the collected measurements, the simulation models were tuned. This allows us to run simulations for various scenarios with validated models and the same conditions (e.g., discharge, head and frequency of the power system). With the hybridization, the total mileage of the guide vanes could be reduced by 43%, while the runner blade's opening movement was reduced by 40.8%. It was quantified that the proportion of mileage that comes from level regulation represents 13.5% for GVO and 24.5% for RBO, respectively. Additionally, a significant reduction in the number of sign changes in the movement of GVO and RBO was observed (number of panel changes by 67% for guide vane openings and 50.7% for runner blade openings).

One boundary condition of the BESS sizing was that the BESS shall reach its end of life at the end of the demonstration phase. However, during the first half of the demonstration phase, the calculated SoH with the BESS was 98%.

Due to the sizing of the BESS (1.8% of the nameplate rating of one unit), the participation in other ancillary services markets is not feasible. However, with a larger BESS rating and capacity, a stand-alone RoR power plant could also participate on intraday and other reserve markets (aFRR, mFRR, etc.).

Until the end of the project, different control strategies will be tested and evaluated in terms of achievable reduction in wear and tear as well as impact on the SoH of the BESS.

Finally, based on the experiences of all demonstrators of the XFLEX HYDRO project, a technical whitepaper and roadmap for the European Hydropower fleet will be published.

Author Contributions: All authors contributed to the paper. All authors have read and agreed to the published version of the manuscript.

Data Availability Statement: Restrictions apply to the availability of the data, due to know how protection. Therefore, the data are not publicly available.

Conflicts of Interest: The authors declare no conflict of interest.

References

1. IHA, International Hydropower Association, 2019 Hydro Power Status Report—Sector Trends and Insights. 2019. Available online: https://www.hydropower.org/sites/default/files/publications-docs/2019_hydropower_status_report.pdf (accessed on 21 May 2019).
2. IRENA. *The Changing Role of Hydropower: Challenges and Opportunities*; International Renewable Energy Agency: Bonn, Germany, 2023.
3. Somani, A.; Datta, S.; Kincic, S.; Chalishazar, V.; Vyakaranam, B.; Samaan, N.; Colotelo, A.; Zhang, Y.; Koritarov, V.; McJunkin, T.; et al. *Hydropower's Contributions to Grid Resilience*; Hydrowires, PNNL-30554; U.S. Department of Energy: Washington, DC, USA, 2021.
4. XFLEX HYDRO—EU Horizon 2020 Project. Available online: https://xflexhydro.net (accessed on 20 January 2020).
5. Frequency Containment Reserves. Available online: https://www.entsoe.eu/network_codes/eb/fcr/ (accessed on 23 May 2023).
6. Datacenter FCR/aFRR/mFRR. Available online: https://www.regelleistung.net/apps/datacenter/tenders/?productTypes=PRL&markets=BALANCING_CAPACITY,BALANCING_ENERGY&date=2023-03-29&tenderTab=PRL$CAPACITY$1 (accessed on 23 May 2023).
7. European Network of Transmission System Operators for Electricity (entso-e). ENTSO-E's Supporting Document to the Submitted Network Code on Load-Frequency Control and Reserves. June 2013. Available online: https://acer.europa.eu/Official_documents/Acts_of_the_Agency/Annexes/ENTSO-E%E2%80%99s%20supporting%20document%20to%20the%20submitted%20Network%20Code%20on%20Load-Frequency%20Control%20and%20Reserves.pdf (accessed on 9 May 2023).
8. Ausschreibungen der Primärregelreserve in der Regelzone APG. Available online: https://www.apg.at/de/markt/netzregelung/primaerregelung/ausschreibungen (accessed on 21 January 2020).
9. Präqualifikationsbedingungen—Regelleistung.net. Available online: https://www.regelleistung.net/ext/static/prequalification (accessed on 29 February 2020).
10. Engels, J.; Claessens, B.; Deconinck, G. Techno-Economic Analysis and Optimal Control of Battery Storage for Frequency Control Services, Applied to the German Market. *Appl. Energy* **2019**, *242*, 1036–1049. [CrossRef]
11. Marchgraber, J.; Gawlik, W.; Alács, C. Modellierung und Simulation von Batteriespeichern bei der Erbringung von Primärregelleistung. *Elektrotech. Inftech.* **2019**, *136*, 3–11. [CrossRef]
12. D7.5—Methodology Report for Application-Specific Design of BESS. *Osmose*. Available online: https://www.osmose-h2020.eu/download/d7-5-methodology-report-for-application-specific-design-of-bess/ (accessed on 28 February 2022).
13. Sandelic, M.; Stroe, D.-I.; Iov, F. Battery Storage-Based Frequency Containment Reserves in Large Wind Penetrated Scenarios: A Practical Approach to Sizing. *Energies* **2018**, *11*, 3065. [CrossRef]
14. Chalishazar, V.H.; Harnish, R.; Bhatnagar, D.; Somani, A.; Bellgraph, B. Hydro-battery Hybrids—A Case for Holistic Assessment of Hybrid Energy Systems. In Proceedings of the IEEE Electrical Energy Storage Application and Technologies Conference (EESAT), Austin, TX, USA, 8–9 November 2022; pp. 1–5. [CrossRef]
15. Bucher, R.; Schreider, A.; Lehmann, S. Live test results of the joint operation of a 12.5 MW battery and a pumped-hydro plant. In Proceedings of the Hydro 2018, Gdanks, Poland, 15–17 October 2018.

16. Kadam, S.; Eiper, T.; Hofbauer, W.; Hell, J. Bereitstellung von Primärregelreserve mit einem Hybridsystem bestehend aus einem Batteriespeicher und einem Laufkraftwerk. In Proceedings of the Symposium Energieinnovation, Graz, Austria, 12–14 February 2020; p. 13.

17. Eiper, T.; Hell, J.; Kadam, S. Hybrid storage systems: Welcome batteries in hydro powerplants. In Proceedings of the Hydro 2019, Porto, Portugal, 14–16 October 2019.

18. Benda, S. Evaluation of Kaplan machinery operating in frequency sensitive mode and derived design specification. In Proceedings of the 19th International Seminar on Hydropower Plants, Flexible Betriebsweise von Wasserkraftanlagen im derzeitigen Energiesystem, Vienna Hydro, Austria, 9–11 November 2016.

19. Wurm, E.; Benda, S. Lebensdauer von Laufradteilen bei unterschiedlichen Betriebsarten von Kaplanturbinen. In Proceedings of the Praktikerkonferenz Wasserkraft, Graz, Austria, 21–22 September 2011.

20. Oram, C. Life time analysis of Kaplan runner mechanism. In Proceedings of the 38th MPA-Seminar, Stuttgart, Germany, 1–2 October 2012.

21. Oberhauser, K.; Stickler, J. Optimised control strategy for primary control with hydropower plants. In Proceedings of the 16th International Seminar on Hydropower Plants, Vienna Hydro, Austria, 24–26 November 2010; Technische Universität Wien, Ed.; Eigenverlag: Wien, Austria; Laxenburg, Austria, 2010; pp. 69–78.

22. Jacqué, K.; Koltermann, L.; Figgener, J.; Zurmühlen, S.; Sauer, D.U. The Influence of Frequency Containment Reserve on the Operational Data and the State of Heal the Hybrid Stationary Large-Scale Storage System. *Energies* **2022**, *15*, 1342. [CrossRef]

23. Benato, R.; Sessa, S.D.; Musio, M.; Palone, F.; Polito, R. Italian Experience on Electrical Storage Ageing for Primary Frequency Regulation. *Energies* **2018**, *11*, 2087. [CrossRef]

24. Ancillary Services Matrix—Stage 2. XFLEX HYDRO—EU Horizon 2020 Project. Available online: https://xflexhydro.net/ancillary-services-matrix-stage-2 (accessed on 26 August 2022).

25. Païs, G.; Vinit, L.; Delaplagne, T.; Montaru, M.; Drommi, J.-L. Hydro power plant hybridization with battery energy storage system for primary frequency control. In Proceedings of the 5th International Hybrid Power Systems Workshop, Virtually, 18–19 May 2021.

26. Gerini, F.; Vagnoni, E.; Cherkaoui, R.; Paolone, M. Improving frequency containment reserve provision in run-of-river hydropower plants. *Sustain. Energy Grids Netw.* **2021**, *28*, 100538. [CrossRef]

27. Drommi, J.-L.; Pais, G.; Nicolet, C.; Landry, C. Increasing flexibility of historical power generation thanks to micro hybrid concept, the Xflex hydro live demonstrator at Vogelgrun HPP. In Proceedings of the CIGRE Session 2022, Paris, France, 28 August–2 September 2022.

28. Nicolet, C.; Bollaert, E. Hydroelectric Power Plant Real-Time Monitoring System and Method. EP2801879A1, 12 November 2014.

29. Nicolet, C.; Bollaert, E. Hydroelectric Power Plant Real-Time Monitoring System and Method. EP3285128B1, 18 November 2020.

30. Nicolet, C.; Dreyer, M.; Béguin, A.; Bollaert, E.; Torrent, S. Hydraulic Transient Survey at Cleuson-Dixence with Real-Time Hydro-Clone Monitoring System. In Proceedings of the Hydro 2018 Conference, Gdansk, Poland, 15–17 October 2018; p. 15.